Atmos. Chem. Phys. Discuss., 6, 8917–8960, 2006
www.atmos-chem-phys-discuss.net/6/8917/2006/

Atmospheric Chemistry and Physics Discussions

Characterization of the ^{222}Rn family turbulent transport in the convective atmospheric boundary layer

J.-F. Vinuesa and S. Galmarini

European Commission – DG Joint Research Centre, Institute for Environment and Sustainability, Italy

Received: 2 June 2006 – Accepted: 26 July 2006 – Published: 25 September 2006

Correspondence to: J.-F. Vinuesa (jeff.vinuesa@jrc.it)

Abstract

The combined effect of turbulent transport and radioactive decay on the distribution of ^{222}Rn and its progeny in convective atmospheric boundary layers (CBL) is investigated. Large eddy simulation is used to simulate their dispersion in steady state CBL and in unsteady conditions represented by the growth of a CBL within a pre-existing reservoir layer.

The exact decomposition of the concentration and flux budget equations under steady state conditions allowed us to determine which processes are responsible for the vertical distribution of ^{222}Rn and its progeny. Their mean concentrations are directly correlated with their half-life, e.g. ^{222}Rn and ^{210}Pb are the most abundant whereas ^{218}Po show the lowest concentrations. ^{222}Rn flux decreases linearly with height and its flux budget is similar to the one of inert emitted scalar, i.e., a balance between on the one hand the gradient and the buoyancy production terms, and on the other hand the pressure and dissipation at smaller scales which tends to destroy the fluxes. While ^{222}Rn exhibits the typical bottom-up behavior, the maximum flux location of the daughters is moving upwards while their rank in the ^{222}Rn progeny is increasing leading to a typical top-down behavior for ^{210}Pb. We also found that ^{222}Rn short-lived daughters, e.g. ^{218}Po and ^{214}Pb, have relevant radioactive decaying contributions acting as flux sources leading to deviations from the linear flux shape. In addition, while analyzing the vertical distribution of the radioactive decay contributions to the concentrations, e.g. the decaying zone, we found a discrepancy in height of ^{222}Rn daughters' radioactive transformations.

Under unsteady conditions, the same behaviors reported under steady state conditions are found: deviation of the fluxes from the linear shape for ^{218}Po, enhanced discrepancy in height of the radioactive transformation contributions for all the daughters. In addition, ^{222}Rn and its progeny concentrations collapse due to the rapid growth of the CBL. The analysis emphasizes the crucial role of turbulent transport in the behavior of ^{222}Rn morning concentrations, in particular the ventilation at the top of the boundary

ACPD

6, 8917–8960, 2006

layer that leads to the dilution of ^{222}Rn by mixing with radon low concentration air.

1 Introduction

^{222}Rn is a natural radioactive compound with a half-life of 3.8 days. Its noble gas nature makes it a suitable tracer in studies of atmospheric boundary layers (Porstendörfer, 1994). Ground-based measurements and vertical distributions of ^{222}Rn and its daughters have been extensively studied in the past, e.g., to characterize the turbulent properties of the ABL, to perform regional and global circulation model benchmarking and to estimate regional surface fluxes of air pollutant and in particular climate-sensitive compounds. For a review on the use of ^{222}Rn observations in atmospheric sciences see Zahorowski et al. (2004). Several authors (Larson et al., 1972; Lopez et al., 1974; Polian et al., 1986; Gaudry et al., 1990; Ramonet et al., 1996; Vinod Kumar et al., 1999) have shown that the study of the behavior of radon and its progeny is of great importance for air pollutant and greenhouse gases transport modeling. In particular, ^{222}Rn is often used to calibrate and validate transport models (Genthon and Armengaud, 1995; Li and Chang, 1996; Jacob et al., 1997; Stockwell et al., 1998; Dentener et al., 1999).

The correlation between ground level radon concentrations and meteorological conditions in the lower atmosphere has been investigated in various occasions (e.g., Moses et al., 1963; Pearson and Moses, 1966; Ikebe, 1970; Druilhet and Fontan, 1973a,b; Beck and Gogolak, 1979; Robé et al., 1992; Kataoka et al., 2001; Galmarini, 2006) including the relationship with the atmospheric stability (e.g., Wilkening, 1970; Guedalia et al., 1974; Fontan et al., 1979; Guedalia et al., 1980; Fujinami and Esaka, 1987; 1988; Kataoka et al., 1998; Sesana et al., 1998). It has also been used to investigate transport processes such as convection (Mahowald et al., 1997; Stockwell et al., 1998; Sesana et al., 2006), diurnal variability (Jacob and Prather, 1990; Kataoka et al., 1998), and synoptic variability of the ABL (Allen et al., 1996). However only few studies have addressed the vertical dispersion of radon and its daughters.

ACPD
6, 8917–8960, 2006

For instance, Ikebe and Shimo (1972), Druilhet and Fontan (1973a,b) and Butterweck et al. (1994) estimated the vertical turbulent diffusivity from ^{220}Rn measurement profiles, Jacobi and Andre (1963) and Beck and Gogolak (1979) evaluated the radon and its daughter products concentration profiles using a local gradient formulation for the fluxes assuming eddy diffusivities to be equal to eddy conductivity. Lopez et al. (1974) and (Guedalia et al., 1973, 1974) used aircraft data to extract information on the vertical transport while Vinod Kumar et al. (1999) used Wangara field experiment data set (Clarke et al., 1971) to analyze their model results.

Some of the radon radionuclides and their short-lived daughters have been used to study the turbulent diffusion process since they have half-lives of the same order of magnitude of the turnover time of the convective boundary layer (CBL). While the so-called long lived species are well mixed and the vertical flux profiles follow a linear shape (Wyngaard, 1985), the short-lived compound fluxes deviate from the inert linear profile. In this respect, accurate modeling requires a better understanding of how turbulence affects the dispersion of ^{222}Rn and its progeny in atmospheric boundary layers. The scales associated with turbulent motions range from the Kolmogorov dissipation scale (on the order of a millimeter) to the boundary layer depth (on the order of a kilometer). The largest eddies are responsible for the turbulent transport of the scalars and momentum whereas the smallest ones are mainly dissipative. Thus, realistic numerical experiments of the atmospheric boundary layer require the use of large-eddy simulation (LES) that allows to explicitly solve relevant turbulent scales.

Previous LES studies have shown that the turbulent mixing can control the concentration and the distribution of reacting scalars in the CBL (Schumann, 1989; Sykes et al., 1994; Gao and Wesely, 1994; Verver et al., 1997; Molemaker and Vilà-Guerau de Arellano, 1998; Petersen et al., 1999; Petersen, 2000; Petersen and Holtslag, 1999; Krol et al., 2000; Patton et al., 2001; Vinuesa and Vilà-Guerau de Arellano, 2003; Vinuesa and Vilà-Guerau de Arellano, 2005). However, these studies have been mostly restricted to moderately fast reacting flows involving a second-order and/or a first order reaction. In particular, Vinuesa and Vilà-Guerau de Arellano (2003) performed a

ACPD
6, 8917–8960, 2006

EGU

budget analysis of the fluxes and (co-)variances for second-order reacting scalars in a steady-state CBL. A key and novel aspect of this work is to extend the analysis to a chain of decaying species with a wide range of half-lives. Every new species decays with a timescale that varies from one to another. Its concentration will depend on its own decay but also on the decay of its mother. Thus the distribution of the new species will be affected by the mixing of the previous one in the chain.

To our knowledge, no study so far has analyzed the turbulent transport of ^{222}Rn short-lived daughters in a CBL in a such comprehensive manner. We perform a complete analysis of the vertical distribution, reactivity and turbulent transport of ^{222}Rn and its progeny under convective conditions. In order to account for all the relevant scales of the atmospheric boundary layer, we use LES to explicitly calculate the different terms of the concentration budget equations. The CBL analyzed here is considered under steady and unsteady conditions i.e. a fully developed CBL and a CBL growing within the reservoir layer resulting from the collapse of previous daytime CBL. In addition to the explicit calculation of the different contributions to concentration budget equations, the study under steady state conditions allows to perform a full budget analysis of the turbulent transport, i.e. the fluxes, and so to identify the driving process of ^{222}Rn and its progeny concentration behavior. The analysis of the unsteady boundary layer aims at understanding the exchanges between the reservoir and the mixed layer while the boundary layer is deepening and so the turbulent timescale is increasing. In addition, the behavior of decaying species in this transient part of the day has never been studied before.

The structure of this paper is as follows. In Sect. 2, we present the chemical system of the ^{222}Rn radioactive decaying chain together with the theoretical basis for concentration and flux budget decompositions. The numerical simulation specifications and the turbulent reacting flow classification are presented in Sect. 3. The vertical distribution, the reactivity and the transport by turbulence of ^{222}Rn and its daughters in the case of the steady-state CBL are analyzed in Sect. 4. In Sect. 5, the results obtained under unsteady conditions are discussed. Finally, a summary is presented and conclu-

ACPD
6, 8917–8960, 2006

sions are drawn in the last section.

2 ^{222}Rn decaying chain

We consider the radioactive decay chain of ^{222}Rn that reads:

$$^{222}\mathrm{Rn} \xrightarrow{\lambda_0} {}^{218}\mathrm{Po} \xrightarrow{\lambda_1} {}^{214}\mathrm{Pb} \xrightarrow{\lambda_2} {}^{214}\mathrm{Bi} \xrightarrow{\lambda_3} {}^{210}\mathrm{Pb}, \quad (1)$$

where λ_0, λ_1, λ_2 and λ_3 are the decay frequencies equal to 2.11×10^{-6}, 3.80×10^{-3}, 4.31×10^{-4}, and 5.08×10^{-4} s^{-1}, respectively. Note that we consider a direct transformation of ^{214}Bi into ^{210}Pb since the half-life of ^{214}Po (daughter of ^{214}Bi) is very short (164 μs). Also we consider ^{210}Pb, that has a half-life of 22.3 years, as an inert scalar with respect to the temporal scales considered here. To increase readability, ^{222}Rn and its progeny will also be referred to as S_i where i is the rank of the daughter in the decay chain from here on, e.g. S_0 and S_4 stand for ^{222}Rn and ^{210}Pb, respectively.

In the planetary boundary layer, under horizontally homogeneous conditions with no mean wind and neglecting the transport due to molecular diffusion, the temporal evolution of the mean concentrations S_i of a radionuclide reads

$$\frac{\partial S_i}{\partial t} = -\frac{\partial \overline{w s_i}}{\partial z} + R_{S_i} \quad (2)$$

where the horizontal averages are denoted both by capital letters and overbars whereas the fluctuations of the variables around the horizontal average value are represented by lower case letters. For the chain (1), the radioactive source/sink terms R_{S_i} are

$$R_{S_0} = -\lambda_0 S_0, \quad (3)$$

$$R_{S_1} = \lambda_0 S_0 - \lambda_1 S_1, \quad (4)$$

$$R_{S_2} = \lambda_1 S_1 - \lambda_2 S_2, \quad (5)$$

ACPD
6, 8917–8960, 2006

EGU

$$R_{S_3} = \lambda_2 S_2 - \lambda_3 S_3, \quad (6)$$

$$R_{S_4} = \lambda_3 S_3. \quad (7)$$

The vertical scalar flux budget equation reads

$$\frac{\partial \overline{w s_i}}{\partial t} = \underbrace{-\overline{w^2}\frac{\partial S_i}{\partial z}}_{G} + \underbrace{\frac{g}{\Theta_0}\overline{\theta s_i}}_{B} \underbrace{-\frac{\partial \overline{w^2 s_i}}{\partial z}}_{T} \underbrace{-\overline{s_i \frac{\partial \pi}{\partial z}}}_{P} \underbrace{-\overline{s_i \frac{\partial \tau_{3j}}{\partial x_j}} - \overline{w \frac{\partial \langle u_j'' s_i'' \rangle}{\partial x_j}}}_{D} + \underbrace{R_{\overline{w s_i}}}_{CH}, \quad (8)$$

where w, θ and s_i represent the fluctuation of the vertical velocity, the temperature and the reactant concentration, respectively. Θ_0 is a reference state potential temperature, S_i is the horizontal average reactant quantity and π is the modified pressure defined as $[(p-p_0)/\rho_0]+(2/3)E$, where p, p_0 and ρ_0 are the pressure, a reference pressure and a reference density respectively, and E is the subgrid-scale turbulent kinetic energy. The subgrid stress for momentum and scalar are represented by τ_{3j} and $\langle u_j'' s_i'' \rangle$ respectively. The terms on the right-hand side are the mean gradient term (G), the buoyancy (B), the turbulent transport (T), the pressure term (P), the dissipation (D) and the chemical or radioactive decay contribution (CH). The description of the flux temporal evolution is of importance to identify the driven processes involved in the turbulent dispersion of ^{222}Rn and its progeny.

The radioactive decay terms in the budget equations are

$$R_{\overline{w s_0}} = -\lambda_0 \overline{w s_0}, \quad (9)$$

$$R_{\overline{w s_1}} = \lambda_0 \overline{w s_0} - \lambda_1 \overline{w s_1}, \quad (10)$$

$$R_{\overline{w s_2}} = \lambda_1 \overline{w s_1} - \lambda_2 \overline{w s_2}, \quad (11)$$

$$R_{\overline{w s_3}} = \lambda_2 \overline{w s_2} - \lambda_3 \overline{w s_3}, \quad (12)$$

$$R_{\overline{w s_4}} = \lambda_3 \overline{w s_3}. \quad (13)$$

ACPD
6, 8917–8960, 2006

3 Description of the numerical simulations

The capacity of LES to simulate extremely accurately turbulent condition of atmospheric boundary layers has been widely proved over the years through extent comparison with laboratory and field measurements. We use the three-dimensional LES code described by Cuijpers and Duynkerke (1993), Siebesma and Cuijpers (1995), Cuijpers and Holtslag (1998) and Vilà-Guerau de Arellano and Cuijpers (2000).

3.1 Specifications of the simulated boundary layers

Two representative cases are investigated: a fully developed free convective atmospheric boundary layer and a CBL growing overlayed by a reservoir layer resulting from the collapse of the previous daytime CBL. For both cases, the modeling domains represent 6.4 km×6.4 km×1.5 km with a vertical and horizontal resolutions of 25 and 50 meters respectively, leading to 128×128×60 grid-points simulations. Periodic lateral boundary conditions are assumed. The maximum time-step used in the calculations is 0.5 s.

The simulated atmospheric boundary layers (ABL) are dry, as radon and its daughters are unaffected by moisture, convective ABLs driven by buoyancy only (see Table 1 and Fig. 1).

In the steady-state CBL, ^{222}Rn is emitted at the surface with a flux of 0.5 Bqm^{-2}s^{-1}. All radioactive compounds have a zero initial profile except ^{222}Rn. The latter is the result of a pre-run of 1 h simulation with the same surface flux, no initial concentration and a decay constant set to zero. The simulation is running for 8 h with a pre-run of 1 h for the dynamics. The statistics and the budget analysis are done on the last hour of the simulation. The convective velocity scale w_*, the ABL height z_i (defined as the depth where the sensible heat flux is minimum) and the free convection time-scale $t_* \equiv z_i/w_*$ are equal to 1.12 ms^{-1}, 800 m and 714.3 s, respectively.

For the unsteady convective BL, we follow a special procedure to initialize ^{222}Rn and its daughters profiles in order to ensure consistency regarding the assumption of

ACPD
6, 8917–8960, 2006

radioactive equilibrium of ^{222}Rn and its progeny. Briefly, the resulting steady-state CBL of the previous simulation is divided into two regions: a nocturnal boundary layer of depth z_{i2} and a reservoir layer. Since the reservoir layer is assumed decoupled from the surface, no fresh radon is transported to this region during the 8-hours' night. In the nocturnal boundary layer, a ^{222}Rn surface flux of 0.5 Bqm^{-2}s^{-1} is assumed constant during the night. In both regions, the ^{222}Rn and its daughters profile concentrations are analytically calculated as the result of a 8 h period of radioactive activity from the resulting profiles of the previously simulated steady-state CBL (see the appendix). The simulation of the unsteady CBL is starting at sunrise and is running for 8 h.

3.2 Reacting turbulent flow classification

The relative influence of turbulence on the species transformations can be quantified by the so-called turbulent Damköhler number Da_t (Damköhler, 1940), defined as the ratio between the integral time-scale of turbulent (τ_t) and the chemical time-scale (τ_c) that is, in this context, the decay time-scale of the radionuclide. Using this number, turbulent reacting flows can be classified into three categories (Schumann, 1989; Molemaker and Vilà-Guerau de Arellano, 1998; Krol et al., 2000; Vilà-Guerau de Arellano, 2003). For reacting flows with $Da_t \ll 1$, the transformation proceeds at a slower rate than the turbulent mixing. Therefore, mixing is reached prior to the transformations. When $Da_t \approx O(1)$, i.e. the time-scale of the transformation is of similar order to the time-scale of the turbulent mixing, atmospheric turbulence controls the transformations. The behavior of active species can differ from the behavior observed and modeled of inert scalars. In the case of a decaying scalar, the effect of turbulent mixing will affect the spatial distribution of the radioactive compounds. For $Da_t \gg 1$, transformations are much faster than the turbulent mixing meaning that species are transformed in-situ and are almost not transported. In our simulations, $\tau_t = z_i / w_*$ and $\tau_c = \lambda_j^{-1}$ with j=0, 1, 2, 3. The corresponding Da_t are summarized in Table 2. These numbers indicate that ^{218}Po (S_1) is strongly influenced by the turbulent mixing of the CBL in both steady and

ACPD
6, 8917–8960, 2006

unsteady conditions. The other short-lived daughters ^{214}Pb (S_2) and ^{214}Bi (S_3) refer to a moderate-slow regime indicating that their distributions are only slightly affected by the combined effects of decay and mixing.

While studying the relevance of accounting for the chemical contribution to second-order moments (fluxes and (co-)variances) of reacting scalars, Vinuesa and Vilà-Guerau de Arellano (2003) extended the turbulent reacting flow classification by deriving other dimensionless numbers, the so-called Damköhler numbers for fluxes and (co-)variances. These numbers use a chemical time-scale based on the chemical terms included in second-order moment budget equations. They showed that for flux and (co-)variance Damköhler numbers $\sim O(1)$, the contribution of chemical terms to second-order moment profiles is significant. The flux Damköhler number can be expressed as the ratio of the flow time-scale to the time-scale of the chemical contribution to the flux. For a scalar B involved the chain

$$A \xrightarrow{\lambda_A} B \xrightarrow{\lambda_B} C, \tag{14}$$

the flux Damköhler number reads

$$Da_{\overline{wb}} = \left| Da_{t,B} - Da_{t,A} \frac{w_* s_{a*}}{w_* s_{b*}} \right| . \tag{15}$$

By using the $w_* s_{i*}$ proposed by Cuijpers and Holtslag (1998), i.e. $w_* s_{i*} = \frac{1}{z_i} \int_0^{z_i} \overline{w s_i} dz$, and chemical time-scales based on the radioactive decaying terms included in flux budget equations, we calculate the flux Damköhler numbers and report them in Table 3. In the steady state CBL, significant effects of the radioactive decay contribution on the flux for ^{218}Po (S_1) and ^{214}Pb (S_2) can be expected whereas ^{214}Bi (S_3) flux Damköhler number only indicates a small contribution of the decaying process. However, under unsteady conditions only ^{218}Po (S_1) flux is affected by the control exerts by turbulence on the radioactive decay contribution.

4 Dispersion of ^{222}Rn and its progeny in the steady-state CBL

4.1 Vertical distribution and radioactive decay contribution

Figure 2 shows the vertical profile of ^{222}Rn and its progeny concentrations. The mixed-layer concentrations are correlated with the half-lives of the compounds; the faster decaying the daughter is, the smaller is the concentration. Also as indicated by the Damköhler number classification, ^{222}Rn concentration only shows a small deviation from the inert scalar one. All the compounds show overall well-mixed profiles however since a wide range of radioactive decay frequencies is considered, e.g. from some minutes to days, any discrepancy in height can have an important impact on the radioactive transformations.

We explicitly calculate the radioactive decay contributions to the concentration budget equations and we show the resulting profiles in Fig. 3. As can be expected for S_0 and since its radioactive decay contribution is proportional to its concentration, the radioactive decay is acting as a sink with a constant value within the mixed layer. For radon's daughters, the radioactive decay terms are composed of a balance between production by the decay of their mother and destruction but their own decay. For all the daughters, the radioactive decay contributions show an unbalance in favor of their production. Thus, as long as S_0 is injected in the steady-state CBL, their concentration will grow with time and this is the direct evidence of the competition between mixing and decaying process. However, one can notice that the daughters' radioactive decay contribution are quite different in the vertical and that, apart R_{S_4} and to some extent R_{S_0}, none of them shows a constant value in the mixed layer.

Since S_1 is the first daughter of the family, its production by the decay of S_0 is more important where the ^{222}Rn concentrations are higher, i.e. close to the surface. The radioactive decay of S_1 proceeds at a faster rate than the turbulent mixing meaning that freshly created S_1 are decaying before being well mixed in the CBL. As a result, the shape of the profile is quite different from the S_0 one showing a fast reduction while

ACPD
6, 8917–8960, 2006

EGU

moving upward. For the daughters with a longer half-life than S_1, turbulence is more efficient to mix freshly created compounds with older ones but still some discrepancy in height can be noted for S_2 and S_3. For the latter, one can notice a very interesting behavior: while all other radioactive contributions are more important close to the surface, the one of S_3 shows a maximum contribution at around 0.6 z/z_i. The decaying term R_{S_3} in the S_3 concentration budget equation is composed of a source term and a sink term. The source term is the production by radioactive decay of S_2, i.e. $\lambda_2\ S_2$, and the sink term is its own radioactive decay, i.e. $\lambda_3\ S_3$. This latter sink term is equal to the radioactive decay contribution R_{S_4}. Since S_4 radioactive decay contribution shows a constant profile at lower altitudes, one can assume that S_3 is well-mixed at these depths. However from the surface to 0.6 z/z_i, R_{S_3} increases suggesting an unbalance between its own radioactive decay and the production by the decay of S_2. Since the radioactive decay of S_2 is proportional to S_2 concentration, we can conclude that S_2 is inefficiently mixed by turbulence and that it has higher concentration at the mid-CBL than at the surface.

As noticed previously, the concentration profiles shown in Fig. 2 look overall well-mixed which can be found discrepant with the inhomogeneous R_{S_i} vertical profiles. However, a closer look to the concentrations or to the concentration gradients for instance (Fig. 4) reveals inhomogeneous mixing of the daughters. While S_1 and S_4 decrease with height, S_2 and S_3 have positive gradients up to the mid-CBL that is in agreement with the analysis of the R_{S_i}. S_1 production is higher close to the emission source of S_0 and since S_1 is transformed at a faster rate than it is transported (with Da_t=2.71), freshly created S_1 are decomposed into S_2 preferentially at around mid-CBL. This clearly shows the relevance of accounting for the influence of turbulent mixing on the dispersion of ^{222}Rn short-lived daughters.

4.2 Turbulent transport

Within the boundary layer, the profiles of inert scalars have a linear shape (Deardorff, 1979; Wyngaard and Brost, 1984; Wyngaard, 1985) whereas the fluxes of re-

acting scalars show deviations with from this shape correlated with their Damköhler numbers (Gao and Wesely, 1994; Sykes et al., 1994; Vinuesa and Vilà-Guerau de Arellano, 2003). These deviations are due to the action of the chemistry that can act as a sink or a source term in the flux budget.

The fluxes of S_0 and its progeny are shown in Fig. 5. The fluxes of S_0 and S_4 have a linear profile whereas the ones of the other daughters show deviations from the linear shape. The flux of ^{222}Rn is similar to an inert scalar flux. Thus the chemical term, that is the radioactive decay in our case, has no impact on the vertical transport of ^{222}Rn as its Damköhler and flux Damköhler numbers suggested with Da_t<0.01 and $Da_{\overline{ws_0}}$<0.01. S_1 has the highest Damköhler number (Da_t=2.71) and its flux shows the biggest deviation. The other short-lived daughters, i.e. S_2 and S_3, have similar Da_t but while the deviation of S_2 flux is significant, the one of S_3 is rather small. Using the appropriate Damköhler number to assess the relevance of radioactive decay contribution to the flux allows clarifying this discrepancy. The flux Damköhler number for S_2 is 0.85 while the one of S_3 equals 0.16 suggesting the vertical transport of S_2 is the one most significantly affected by turbulence.

The most interesting point is that the vertical distribution of the fluxes changes from one daughter to another. For S_0, the maximum flux is found at the surface where it is emitted. Since all daughters are produced by the radioactive decomposition of S_0, one would expect to find maximum daughter fluxes close to the surface. However and as can be clearly noticed in Fig. 5, this is not the case and the maximum flux location is moving upwards while the rank of the daughter in the ^{222}Rn progeny is increasing. S_1 has its maximum flux at 0.25 z/z_i and the others daughters maximum fluxes are located around 0.9 z/z_i. Actually, the maximum flux location reaches a quasi steady state value betwen 0.90 and 0.95 z/z_i for the slowest (in the flux Damköhler number sense) daughters, i.e., S_3 and S_4.

The understanding of the changes of flux profile shape behaviors through ^{222}Rn progeny requires the determination of which physical processes are responsible for their fluxes. Therefore, in order to study the relevance of the radioactive decay con-

tribution to the flux, the terms of the flux budget equation (8) have been calculated explicitly. For an inert emitted scalar, our results are similar to previous studies (Deardorff, 1974; Moeng and Wyngaard, 1984) and will not be presented here. Briefly, the budget for inert emitted scalar reveals a balance between the gradient and the buoyancy production terms on the one hand, which are the major flux sources up to the middle of the boundary layer, and on the other hand the pressure and dissipation at smaller scales which tend to destroy the fluxes. The transport contribution is removing flux from the lower boundary layer upwards with a maximum dissipating effect close to the surface.

Figure 6 shows the vertical profiles of the different contribution to the fluxes of S_0 and S_4. Both have a negligible radioactive decay contribution. S_0 flux show the typical decomposition obtained for bottom-up inert scalar (with a maximum flux at the surface) and S_4 flux shows the one of a top-down inert scalar (with a maximum flux at the top of the CBL). For this latter, we found similar results to the work of Cuijpers and Holtslag (1998) and in particular their case *a*1. The gradient contribution becomes very small in the lower boundary layer where the main production due to buoyancy is balanced by the pressure correlation and the turbulent transport contributions. Turbulent transport is transporting flux upward with its maximum dissipative contribution is located around 0.8 z/z_i. For S_0 and S_4, accounting for the radioactive decay contribution to the flux is not relevant as was suggested by their very low flux Damköhler numbers (Table 3).

In Fig. 7, the vertical contributions to the flux budget equations of the other daughters are presented. We found that the radioactive decay term is responsible for a relevant part of the flux production for S_1 and S_2 whereas it is almost negligible for S_3. This is again in agreement with the flux Damköhler numbers presented in Table 3. The gradient production, i.e., $\overline{w^2}\frac{\partial S_i}{\partial z}$, is the most affected term meaning that the radioactive decay is responsible for the decrease of the concentration gradient. The gradient term is reduced to one half of the S_0 value and equals the radioactive decay contribution in the lower boundary layer in the case of S_1. In the S_2 flux budget, it is actually dissipating

flux in the same region. Its contribution becomes small but remains negative for S_3 and it reaches a zero contribution for S_4 (see Fig. 6 of this paper and Fig. 3c of Cuijpers and Holtslag, 1998, to compare to a top-down inert scalar). The other term that is showing differences while comparing flux budget contribution from the daughters is the turbulent transport contribution, i.e., $\frac{\partial \overline{w^2 s_i}}{\partial z}$. In the case of S_1 the turbulent transport is extracting more flux from the lowest levels while for S_2 and S_3 the transport has an almost constant dissipating contribution for all levels below 0.8 z/z_i.

The results shown in Figs. 6 and 7 suggest that the radioactive decay is primarily acting on the concentration gradients leading to an important reduction of the gradient contribution to the flux and even a change of the contribution, i.e. to production from dissipation, especially for S_2. To a less important extent, the turbulent transport is also affected showing an enhancement of the transfer of flux from the lower levels to the top of the CBL.

These findings combined with the analysis of the radioactive contributions to the evolution of the mean concentrations presented in Fig. 3 lead to the conclusion that atmospheric turbulence controls the distribution of S_1, S_2 and S_3.

5 Dispersion of ^{222}Rn and its progeny under unsteady conditions

In this section, we extend our analysis to atmospheric boundary layers under unsteady conditions focusing on a CBL growing within an overlayed reservoir layer. Our study aims at understanding the exchanges between the reservoir and the mixed layer while the boundary layer is deepening (from 187.5 m to 600 m) and so the turbulent timescale is increasing (from 306.5 s to 605.9 s). In addition, the behavior of decaying or reacting species in this transient part of the day has never been fully studied before.

ACPD
6, 8917–8960, 2006

EGU

5.1 Vertical distribution

In Fig. 8, we show the time evolution of the concentration of the mother ^{222}Rn (S_0) and the last daughter of the chain ^{210}Pb (S_4). The other daughters are not shown since they have the same overall behavior as S_0. No fresh emissions of S_0 reach the reservoir layer since it is almost decoupled from the surface. As a result, S_0 (and the other daughters except S_4) concentration decreases with time. Since S_4 is the last daughter of the chain and is considered as an inert scalar, its concentration increases with time following the chain decaying process.

As the boundary layer deepens with time, the S_0 mixed-layer concentration collapses despite of fresh emission. This collapse is due to both the dilution of S_0 in an increasing volume and the entrainment of S_0 low concentration air from the reservoir layer. The same behavior is observed for the other daughters (except S_4 that shows CBL concentrations enhancing with time). Their concentrations are the result of antagonist effects: the production by the decaying chain, the dilution by boundary layer deepening and the ventilation due to the entrainment of lower concentration air masses from the reservoir layer. The production by the radioactive decay contribution is not sufficient to balance the dilution and the ventilation leading to a decrease of the mixed-layer concentrations. However, in the case of S_4, one can notice that its concentration increases in the reservoir layer since it is considered as an inert and thus as the last product of the decaying chain. This increase limits the ventilation effect due to vertical transport at the entrainment layer. In this case, the combined effect of dilution and detrainment do not balance the production by the radioactive decay and, as a result, S_4 concentration increases with time in the CBL.

5.2 Radioactive decay and turbulent transport contributions

The time evolution of the concentrations is the result of the combined effect of the divergence of the fluxes that is the contribution of the turbulent transport, and the radioactive decay contribution (2). In order to understand which process is responsible

for the collapse of the ^{222}Rn and its short-lived daughters concentration in unsteady atmospheric boundary layers, we focus in the following on the vertical profiles of the radioactive decay contributions (Fig. 9) and fluxes (Fig. 10).

Under unsteady conditions, we found similar vertical profiles of the radioactive decay contribution to S_0 progeny concentrations as we found previously for the fully developed CBL. The radioactive decay term acts as a sink for S_0 and as a source for its progeny. Moreover, the same discrepancy in height can be reported. All contributions show a maximum close to the surface except R_{S_3} and R_{S_4}. While the radioactive decay contribution to S_3 concentration is maximum at the mid-CBL, R_{S_4} shows a well-mixed profile. Also a fast reduction of the decay contribution to S_2 is found while moving upward.

However, the discrepancy with height of the radioactive decay contributions is enhanced while the boundary layer is deepening. As suggested by their turbulent Damköhler numbers shown in Table 2, S_1, S_2 and S_3 are affected by the turbulent structures. Moreover since the Da_t are proportional to τ_t, the Da_t increase together with the turbulent timescale. When the turnover time of the CBL is increasing, it takes more time for turbulence to transport and mix the compounds all over the boundary layer. As a result, the turbulent mixing of radon's daughters is less efficient and the discrepancy with height of the radioactive contribution is increasing with time.

Figure 10 shows the time evolution of the vertical fluxes for S_0, and S_1. The fluxes of the other daughters are not shown since they have similar shape as the ones of S_1. Actually for S_2 and its daughters, we found the same behavior reported for the steady-state CBL: linear shapes (as suggested by the flux Damköhler numbers given in Table 3) with their maximum located close to the top of the boundary layer. Also suggested by the flux Damköhler numbers, only S_1 fluxes show deviation from the inert shape and these deviations are decreasing with time as do the flux Damköhler numbers (from $Da_{\overline{ws_1}}$=0.62 at the beginning of the simulation to $Da_{\overline{ws_1}}$=0.38 at the end).

The most remarkable difference with the steady-state case is the behavior of S_0. In the steady-state CBL, S_0 flux is a bottom-up flux with a maximum value at the surface

ACPD
6, 8917–8960, 2006

EGU

(Fig. 5) whereas under unsteady conditions, the maximum S_0 flux is moving toward the boundary layer top (Fig. 10a). Actually, the flux shows maximum values when the boundary layer growth rate is maximum. While the boundary layer is deepening, low ^{222}Rn concentration air masses are entrained from the reservoir layer. Turbulence transport is balancing the gradient of concentration induced by the entrainment of cleaner air by transporting ^{222}Rn towards the upper boundary layer. This upward flux is more vigorous when the ventilation process is enhanced by the increase of the boundary layer growth rate. Thus, the driving process responsible for the collapse of S_0 concentration is much more likely the ventilation due to the entrainment of low-concentration air masses from the reservoir layer.

5.3 Role of entrainment on ^{222}Rn mixed-layer concentration

We have seen previously that entrainment plays a crucial role on the behavior of ^{222}Rn and its progeny morning concentrations. The entrainment fluxes $(\overline{ws_i})_e$ account for the exchange of compounds between the boundary layer and the free troposphere (or here the reservoir layer) and thus influence the vertical distribution of ^{222}Rn and its daughters in the lower part of the troposphere. In the following, we focus on the entrainment flux to the surface flux ratio of ^{222}Rn, i.e. $\beta_0 = \frac{-(\overline{ws_0})_e}{(\overline{ws_0})_s}$ where $(\overline{ws_0})_e$ and $(\overline{ws_0})_s$ are the entrainment and surface flux of S_0 respectively, to outline the importance of the entrainment process. Figure 11 shows the time evolution of β (the ratio of entrainment to the surface flux of potential temperature), β_0 and the mixed-layer concentration $<S_0>$.

The calculation of β gives an almost constant value of $\beta = 0.2$ throughout the whole period of simulation. The β ratio is similar to other results obtained for CBLs simulated by a large-eddy simulation, moreover these studies show values ranging from 0.2 to 0.25 for buoyancy driven atmospheric boundary layers (van Zanten et al., 1999). The β values indicate that the turbulent eddies entrain warmer air from the free troposphere into the ABL. Since the reservoir layer concentrations are lower than the mixed layer ones, the entrained air is also cleaner (with lower concentrations of ^{222}Rn and its

ACPD
6, 8917–8960, 2006

EGU

progeny).

The β ratios for ^{222}Rn are ranging from β_0=−0.5 to β_0=−2 and exhibits a maximum in absolute value at the time of the maximum growth of the boundary layer (at around t=300 min). The sign of the β_0 indicates that, since ^{222}Rn is emitted at the surface, the surface and the entrainment fluxes are both upward fluxes and so reveals the importance of the ventilation process at the top of the CBL. As can be clearly seen in Fig. 11b, the ^{222}Rn mixed-layer concentration $<S_0>$ exhibits two distinct periods. The first one (until 120 min) is characterized by the dominance of the emission from the surface (with $|\beta_0| \leq 1$) and by the growth of the mixed layer concentration. During the second period (after 2 h of simulation), the concentration is decreasing despite of the constant emission of ^{222}Rn at the surface and the β_0 show absolute values greater than 1. This correlation between the mixed layer concentration and β_0 indicates that the main process responsible for the decrease of $<S_0>$ is the mixing with low ^{222}Rn concentration air originating from the reservoir layer. In other words, the ventilation induced by the deepening of the boundary layer enhances the entrainment flux leading to a decrease of the mixed layer concentration.

6 Summary and conclusions

The capacity of large-eddy simulation to perform accurate simulations of turbulent atmospheric boundary layers has been used to provide a complete and comprehensive analysis of the effect of turbulent transport on the distribution of ^{222}Rn and its progeny. Studying how turbulent mixing controls the concentration and the distribution of decaying species with a wide range of half-lives allowed us to address the full range of atmospheric turbulent reacting flow, from slow to fast chemical regimes. Two representative cases are investigated: a steady state free convective atmospheric boundary layer and a CBL growing within a pre-existing reservoir layer.

Under steady state conditions, this analysis revealed that the concentrations are correlated with the half-life of the radioactive compounds and that the short-lived daugh-

ters' vertical distribution can be affected by the turbulent structure of the atmospheric boundary layer. While focusing on the radioactive decay contributions to the concentrations, we found an important discrepancy in height for the short-lived daughters. This leads to the conclusion that since the radioactive decay considered covers wide range of frequencies, even small discrepancies in the vertical distribution of the concentrations can have important impact on the radioactive transformations due to the inefficient mixing of turbulence. In particular, the radioactive decay contribution to ^{214}Bi exhibits a maximum far away from the surface where the radioactive decay contributions to the other daughters concentrations are maximum. This maximum is 5% higher than the contribution calculated at the surface. We showed that this profile was the result of the unability of turbulence to mix efficiently both ^{218}Po and ^{214}Pb in the CBL.

In addition, the fluxes of ^{222}Rn and ^{210}Pb have a linear profile whereas the ones of the other daughters show deviations from the linear shape. The deviations are due to the radioactive decaying process that acts as a source term in the flux budget. Using the appropriate Damköhler number, i.e. flux Damköhler number, assessed the relevance of radioactive decay contribution to the flux. Also it allowed to classified accurately the daughters with respect to the effect of turbulent mixing on their vertical transport, e.g. ^{214}Pb and ^{214}Bi have similar decay frequencies but only ^{214}Pb is significantly affected by turbulence. The exact decomposition of the flux budget reveals that while ^{222}Rn shows the typical bottom-up scalar flux behavior, the last daughter ^{210}Pb exhibits the one of a top-down scalar. We also found that ^{222}Rn short-lived daughters, e.g. ^{218}Po and ^{214}Pb, have relevant radioactive decaying contributions to their fluxes acting as sources leading to deviations from the linear flux shape as suggested by their flux Damköhler numbers. This analysis was confirmed by the explicit calculation of the different contributions to the flux budget equation. We also found that the gradient contribution to the flux is the most affected term meaning that the radioactive decay process is primaly responsible for the relative decrease of the concentration gradient.

The combined budget analysis of the turbulent transport and the radioactive decay of ^{222}Rn progeny in the steady state CBL clearly showed the relevance of accounting

ACPD
6, 8917–8960, 2006

EGU

for the influence of turbulent mixing on the dispersion of ^{222}Rn and its progeny.

Under unsteady conditions, ^{222}Rn and its progeny concentrations (except ^{210}Pb) collapse due to the growth of the boundary layer. We found similar behaviors as in the steady state CBL for the radioactive decay contributions to the concentrations with, however, an enhancement of the discrepancy in height while the boundary layer is deepening. This deepening leads to the increase of the turnover time of the CBL. Therefore it takes more time for turbulence to transport and mix the compounds all over the boundary layer. The fluxes are also affected by the deepening of the CBL. In particular, while ^{222}Rn flux is maximum at the surface in the fully developed CBL, it is moving upwards under unsteady conditions and reaches a maximum for the fastest boundary layer growth. The analysis of the entrainment flux to the surface flux ratio correlated to the mixed-layer concentration of ^{222}Rn showed that the growth of the boundary layer is inducing ventilation at the top of the CBL that entrains cleaner air from the reservoir layer resulting in the collpase of the mixed layer concentration.

The boundary layer concentration of ^{222}Rn is the result of the balance between production by emission at the surface, destruction by radioactive decay, dilution by boundary layer deepening and ventilation due to the entrainment of low-concentration air from the free troposphere. In the morning while the boundary layer is growing, the main process responsible for ^{222}Rn concentration behavior is the ventilation while when the boundary layer is fully developed, the destruction by radioactive decay becomes the preponderant sink for the concentration.

From this comprehensive study, we can conclude that the turbulent properties of the atmospheric convective boundary layers are relevant for studying the dispersion and the transport of the ^{222}Rn family. Therefore accurate modeling requires accounting for the turbulent properties of the ABL. Finally, the turbulent and flux Damköhler numbers have shown to be usefull dimensionless numbers to classify the effects of turbulent mixing on the concentration and the vertical transport of reacting scalars.

ACPD
6, 8917–8960, 2006

EGU

Appendix A

Analytical solution for ^{222}Rn and its pregony concentrations

For the chain of reactions

$$A \xrightarrow{\lambda_1} B \xrightarrow{\lambda_2} C \xrightarrow{\lambda_3} D \xrightarrow{\lambda_4} E, \tag{A1}$$

the chemical system that has to be solved is

$$\frac{dA}{dt} = -\lambda_1 A, \tag{A2}$$

$$\frac{dB}{dt} = \lambda_1 A - \lambda_2 B, \tag{A3}$$

$$\frac{dC}{dt} = \lambda_2 B - \lambda_3 C, \tag{A4}$$

$$\frac{dD}{dt} = \lambda_3 C - \lambda_4 D, \tag{A5}$$

$$\frac{dE}{dt} = \lambda_4 D. \tag{A6}$$

For such a system with a_0, b_0, c_0, d_0 and e_0 as initial concentrations of A, B, C, D and E respectively, the analytical solutions read

$$A = a_0 e^{-\lambda_1 t}, \tag{A7}$$

$$B = b_0 e^{-\lambda_2 t} + \frac{a_0 \lambda_1}{(\lambda_2 - \lambda_1)} \left(e^{-\lambda_1 t} - e^{-\lambda_2 t} \right), \tag{A8}$$

ACPD
6, 8917–8960, 2006

EGU

$$C = c_0 e^{-\lambda_3 t} + \frac{a_0 \lambda_1 \lambda_2}{(\lambda_3 - \lambda_1)(\lambda_2 - \lambda_1)} \left(e^{-\lambda_1 t} - e^{-\lambda_3 t} \right) + \frac{\lambda_2}{(\lambda_3 - \lambda_2)} \left(b_0 - \frac{a_0 \lambda_1}{(\lambda_2 - \lambda_1)} \right) \left(e^{-\lambda_2 t} - e^{-\lambda_3 t} \right), \quad \text{(A9)}$$

$$D = d_0 e^{-\lambda_4 t} + \frac{a_0 \lambda_1 \lambda_2 \lambda_3}{(\lambda_4 - \lambda_1)(\lambda_3 - \lambda_1)(\lambda_2 - \lambda_1)} \left(e^{-\lambda_1 t} - e^{-\lambda_4 t} \right) + \frac{\lambda_2 \lambda_3}{(\lambda_4 - \lambda_2)(\lambda_3 - \lambda_2)} \left(b_0 - \frac{a_0 \lambda_1}{(\lambda_2 - \lambda_1)} \right) \left(e^{-\lambda_2 t} - e^{-\lambda_4 t} \right) + \left[c_0 - \frac{a_0 \lambda_1 \lambda_2}{(\lambda_3 - \lambda_1)(\lambda_2 - \lambda_1)} - \frac{\lambda_2}{(\lambda_3 - \lambda_2)} \left(b_0 - \frac{a_0 \lambda_1}{(\lambda_2 - \lambda_1)} \right) \right] \times \frac{\lambda_3}{(\lambda_4 - \lambda_3)} \left(e^{-\lambda_3 t} - e^{-\lambda_4 t} \right), \quad \text{(A10)}$$

$$E = e_0 + (a_0 - A) + (b_0 - B) + (c_0 - C) + (d_0 - D). \quad \text{(A11)}$$

These analytical solutions have been used to initialize the vertical profiles of ^{222}Rn and its progeny in the reservoir layer for the unsteady condition simulation. In the nocturnal boundary layer (NBL), ^{222}Rn is continuously emitted at the surface and is assumed to be instantaneously mixed within the NBL of depth z_i. In the previous system, this situation corresponds to the injection of fresh material of A, thus A time evolution concentration now read

$$\frac{dA}{dt} = -\frac{\left(F_{z_i} - F_s \right)}{z_i} - \lambda_1 A, \quad \text{(A12)}$$

ACPD
6, 8917–8960, 2006

where the vertical flux divergence is approximated by the ratio of the net flux, i.e. the difference between the surface flux F_s and the detrainment flux at the top of the CBL F_{z_i}, to the boundary layer depth z_i. Assuming that $F_{z_i} \ll F_s$, the analytical solutions of the system become

$$A = \frac{F_s}{\lambda_1 z_i} + \alpha e^{-\lambda_1 t}, \tag{A13}$$

$$B = \frac{F_s}{\lambda_2 z_i} + \beta e^{-\lambda_2 t} + \frac{\alpha\lambda_1}{(\lambda_2 - \lambda_1)}\left(e^{-\lambda_1 t} - e^{-\lambda_2 t}\right), \tag{A14}$$

$$\begin{aligned} C = {} & \frac{F_s}{\lambda_3 z_i} + \chi e^{-\lambda_3 t} + \frac{\alpha\lambda_2\lambda_1}{(\lambda_3 - \lambda_1)(\lambda_2 - \lambda_1)}\left(e^{-\lambda_1 t} - e^{-\lambda_3 t}\right) \\ & + \frac{\lambda_2}{(\lambda_3 - \lambda_2)}\left(\beta - \frac{\alpha\lambda_1}{(\lambda_2 - \lambda_1)}\right)\left(e^{-\lambda_2 t} - e^{-\lambda_3 t}\right), \end{aligned} \tag{A15}$$

$$\begin{aligned} D = {} & \frac{F_s}{\lambda_4 z_i} + \delta e^{-\lambda_4 t} + \frac{\alpha\lambda_3\lambda_2\lambda_1}{(\lambda_4 - \lambda_1)(\lambda_3 - \lambda_1)(\lambda_2 - \lambda_1)}\left(e^{-\lambda_1 t} - e^{-\lambda_4 t}\right) \\ & + \frac{\lambda_3\lambda_2}{(\lambda_4 - \lambda_2)(\lambda_3 - \lambda_2)}\left[\beta - \frac{\alpha\lambda_1}{(\lambda_2 - \lambda_1)}\right]\left(e^{-\lambda_2 t} - e^{-\lambda_4 t}\right) \\ & + \left[\chi - \frac{\alpha\lambda_2\lambda_1}{(\lambda_3 - \lambda_1)(\lambda_2 - \lambda_1)} - \frac{\lambda_2}{(\lambda_3 - \lambda_2)}\left(\beta - \frac{\alpha\lambda_1}{(\lambda_2 - \lambda_1)}\right)\right] \\ & \times \frac{\lambda_3}{(\lambda_4 - \lambda_3)}\left(e^{-\lambda_3 t} - e^{-\lambda_4 t}\right), \end{aligned} \tag{A16}$$

ACPD
6, 8917–8960, 2006

EGU

$$
\begin{aligned}
E = e_0 + \frac{F_s}{z_i}t + \frac{\alpha\lambda_4\lambda_3\lambda_2}{(\lambda_4-\lambda_1)(\lambda_3-\lambda_1)(\lambda_2-\lambda_1)}\left(e^{-\lambda_1 t}-1\right) \\
+\frac{\lambda_4\lambda_3}{(\lambda_4-\lambda_2)(\lambda_3-\lambda_2)}\left(\beta-\frac{\alpha\lambda_1}{(\lambda_2-\lambda_1)}\right)\left(e^{-\lambda_2 t}-1\right) \\
+\frac{\lambda_4}{(\lambda_4-\lambda_3)}\left[\chi-\frac{\alpha\lambda_2\lambda_1}{(\lambda_3-\lambda_1)(\lambda_2-\lambda_1)}-\frac{\lambda_2}{(\lambda_3-\lambda_2)}\left(\beta-\frac{\alpha\lambda_1}{(\lambda_2-\lambda_1)}\right)\right]\left(e^{-\lambda_3 t}-1\right) \\
-\left(\frac{\lambda_3\lambda_2}{(\lambda_4-\lambda_2)(\lambda_3-\lambda_2)}\left(\beta-\frac{\alpha\lambda_1}{(\lambda_2-\lambda_1)}\right)+\frac{\alpha\lambda_3\lambda_2\lambda_1}{(\lambda_4-\lambda_1)(\lambda_3-\lambda_1)(\lambda_2-\lambda_1)}\right. \\
\left.+\frac{\lambda_3}{(\lambda_4-\lambda_3)}\left[\chi-\frac{\alpha\lambda_2\lambda_1}{(\lambda_3-\lambda_1)(\lambda_2-\lambda_1)}-\frac{\lambda_2}{(\lambda_3-\lambda_2)}\left(\beta-\frac{\alpha\lambda_1}{(\lambda_2-\lambda_1)}\right)\right]+\delta\right) \\
\times\left(e^{-\lambda_4 t}-1\right), \qquad \text{(A17)}
\end{aligned}
$$

where

$$
\begin{aligned}
\alpha &= a_0 - \frac{F_s}{\lambda_1 z_i}, \\
\beta &= b_0 - \frac{F_s}{\lambda_2 z_i}, \\
\chi &= c_0 - \frac{F_s}{\lambda_3 z_i}, \\
\delta &= d_0 - \frac{F_s}{\lambda_4 z_i}. \qquad \text{(A18)}
\end{aligned}
$$

Acknowledgements. All computations were performed on the Linux cluster of the ECOMAR action of the Institute for Environment and Sustainability. The authors wish to thank A. Stips and P. Simons who kindly provided the access to this facility.

References

Allen, D. J., Rood, R. B., Thompson, A. M., and Hudson, R. D.: Three-dimensional radon-222 calculations using assimilated meteorological data and a convective mixing algorithm, J. Geophys. Res., 101, 6871-6881, 1996. 8919

Beck, H. L. and Gogolak, C. V.: Time dependent calculation of the vertical distribution of 222Rn and its decay products in the atmosphere, J. Geophys. Res., 84, 3139–3148, 1979. 8919, 8920

Butterweck, G., Reineking, A., Kesten, J., and Porstendörfer, J.: The use of the natural radioactive noble gases radon and thoron as tracers for the study of the turbulent exchange in the atmospheric boundary layer - case study in and above a wheat field, Atmos. Environ., 28, 1963-1969, 1994. 8920

Clarke, R. H., Dyer, A. J., Brook, R. R., Reid, D. G., and Troup, A. J.: The Wangara experiment: boundary layer data, Paper No. 19, Div. of Meteorol. Physics, CSIRO, Australia, 1971. 8920

Cuijpers, J. W. M. and Duynkerke, P. G.: Large eddy simulations of trade wind with cumulus clouds, J. Atmos. Sci., 50, 3894–3908, 1993. 8924

Cuijpers, J. W. M. and Holtslag, A. A. M.: Impact of skewness and nonlocal effects on scalar and buoyancy fluxes in convective boundary layers, J. Atmos. Sci., 55, 151–162, 1998. 8924, 8926, 8930, 8931, 8954

Damköhler, G.: Influence of turbulence on the velocity flames in gas mixtures, Z. Elektrochem., 46, 601–626, 1940. 8925

Deardorff, J. W.: Three-dimensional numerical study of turbulence in an entraining mixed layer, Bound.-Layer Meteorol., 7, 199–226, 1974. 8930

Deardorff, J. W.: Prediction of convective mixed-layer entrainment for realistic capping inversion structure, J. Atmos. Sci., 36, 424–436, 1979. 8928

Dentener, F., Feichter, J., and Jeuken, A.: Simulation of the transport of Rn-222 using on-line and off-line global models at different horizontal resolutions: a detailed comparison with measurements, Tellus 51B, 573–602, 1999. 8919

Druilhet, A. and Fontan, J.: Détermination des coefficients de diffusion verticale entre 0 et 100 m à l'aide du radon et du ThB, Bound.-Layer Meteorol., 3, 468-498, 1973a. 8919, 8920

Druilhet, A. and Fontan, J.: Utilisation du thoron pour la détermination du coefficient vertical de diffusion turbulante près de sol, Tellus 25, 199-212, 1973b. 8919, 8920

Fontan, J., Guedalia, D., Druilhet, A., and Lopez, A.: Une méthode de mesure de la stabilité

verticale de latmosphère près du sol, Bound.-Layer Meteorol., 17, 3–14, 1979. 8919
Fujinami, N. and Esaka, S.: Variations in Radon 222 daughter concentrations in surface air with atmospheric stability, J. Geophys. Res., 92, 1041–1043, 1987. 8919
Fujinami, N. and Esaka, S.: A simple model for estimating the mixing depth from the diurnal variation of atmospheric 222Rn concentration, Rad. Prot. Dos., 24, 88–91, 1988. 8919
Galmarini, S.: One year of 222-Rn concentration in the atmospheric surface layer, Atmos. Chem. Phys., 6, 2865–2887, 2006. 8919
Gao, W. and Wesely, M. L.: Numerical modelling of the turbulent fluxes of chemically reactive trace gases in the atmospheric boundary layer, J. Appl. Meteorol., 33, 835–847, 1994. 8920, 8929
Guedalia, D., Allet, C., Fontan, J., Druilhet, A., and Assaf, G.: Lead-212, Rn, and vertical mixing in the lower atmosphere (100-2000 m), Tellus 25, 381-385, 1973. 8920
Guedalia, D., Allet, C., and Fontan, J.: Vertical exchange measurements in the lower troposphere using ThB (212Pb) and radon (222Rn), J. Appl. Meteorol., 13, 27-39, 1974. 8919, 8920
Guedalia, D., N'Tsila, A., Druilhet, A., and Fontan, J.: Monitoring of the atmospheric stability above an urban and suburban site using rodar and radon measurements, J. Appl. Meteorol., 19, 839-848, 1980. 8919
Gaudry, A., Polian, G., Ardouin, B., and Lambert, G.:Radon-calibrated emissions of CO2 from South Africa, Tellus 42B, 9-19, 1990. 8919
Genthon, C. and Armengaud, A.: Radon-222 as a comparative tracer of transport and mixing in 2 general-circulation models of the atmosphere, J. Geophys. Res., 100, 2849–2866, 1995. 8919
Ikebe, Y.: Variation of radon and thoron concentrations in relation to the wind speed, J. Meteorol. Soc. Jpn., 48, 461-467, 1970. 8919
Ikebe, Y. and Shimo, M.: Estimation of the vertical turbulent diffusivity from thoron profiles, Tellus 24, 29-37, 1972. 8920
Jacob, D. J. and Prather, M. J.: Radon-222 as a test of convective transport in a general circulation model, Tellus 42B, 118-134, 1990. 8919
Jacob, D. J., Prather, M. J., Rasch, P. J., Shia, R. L., Balkanski, Y. J., Beagley, S. R., Bergmann, D. J., Blackshear, W. T., Brown, M., Chiba, M., Chipperfield, M. P., deGrandpre, J., Dignon, J. E., Feichter, J., Genthon, C., Grose, W. L., Kasibhatla, P. S., Kohler, I., Kritz, M. A., Law, K., Penner, J. E., Ramonet, M., Reeves, C. E., Rotman, D. A., Stockwell, D. Z., VanVelthoven, P.

F. J., Verver, G., Wild, O., Yang, H., and Zimmermann, P.: Evaluation and intercomparison of global atmospheric transport models using Rn-222 and other short-lived tracers, J. Geophys. Res., 102, 5953–5970, 1997. 8919

Jacobi, W. and Andre, K.: The vertical distribution of 222Rn, 220Rn and their decay products in the atmosphere, J. Geophys. Res., 68, 3799–3814, 1963. 8920

Kataoka, T., Yunoki, E., Shimizu, M., Mori, T., Tsukamoto, O., Ohhashi, Y., Sahashi, K., Maitani, T., Miyashita, K., Fujikawa, Y., and Kudo, A.: Diurnal variation in radon concentration and mixing-layer gepth, Bound.-Layer Meteorol., 89, 225-250, 1998. 8919

Kataoka, T., Yunoki, E., Shimizu, M.,Mori, T., Tsukamoto, O., Ohhashi, Y., Sahashi, K., Maitani, T.,Miyashita, K., Iwata, T., Fujikawa, Y., Kudo, A., and Shaw, R. H.: A study of the atmospheric boundary layer using raon and air pollutants as tracers, Bound.-Layer Meteorol., 101, 131-155, 2001. 8919

Krol, M. C., Molemaker, M. J., and Vilà-Guerau de Arellano, J.: Effects of turbulence and heterogeneous emissions on photochemically active species in the convective boundary layer, J. Geophys. Res., 105, 6871–6884, 2000. 8920, 8925

Larson, R. E., Lamontagne, R. A., and Wittmann, W. I.: Radon-222, CO, CH4 and continental dust over the greenland and norwegian seas, Nature, 240, 345-347, 1972. 8919

Li, Y. H. and Chang, J. S.: A three-dimensional global episodic tracer transport model. 1. Evaluation of its processes by radon 222 simulations, J. Geophys. Res., 101, 25 931–25 947, 1996. 8919

Lopez, A., Guedalia, D., Servant, J., and Fontan, J.: Advantages of the use of radioactive tracers 222Rn and 212Pb for the study of aitken nuclei within the lower troposphere, J. Geophys. Res., 79, 1243-1252, 1974. 8919, 8920

Mahowald, N. M., Rasch, P. J., Eaton, B. E., Whittlestone, S., and Prinn, R. G.: Transport of (222)radon to the remote troposphere using the model of atmospheric transport and chemistry and assimilated winds from ECMWF and the National Center for Environmental Prediction NCAR, J. Geophys. Res., 102, 28 139-28 151, 1997. 8919

Moeng, C. H. and Wyngaard, J. C.: Statistics of conservative scalars in the convective boundary layer, J. Atmos. Sci., 41, 3161–3169, 1984. 8930

Molemaker, M. J. and Vilà-Guerau de Arellano, J.: Turbulent control of chemical reactions in the convective boundary layer, J. Atmos. Sci., 55, 568–579, 1998. 8920, 8925

Moses, H., Lucus Jr., H. F., and Zerbe, G. A.: The Effect of Meteorological Variables upon Radon concentration three feet above the ground, J. Air Pollut. Control. Assoc., 13, 12-19,

1963. 8919
Patton, E. G., Davis, K. J., Barth, M. C., and Sullivan, P. P.: Decaying scalars emitted by a forest canopy: a numerical study, Bound.-Layer Meteorol., 100, 91–129, 2001. 8920
Pearson, J. E. and Moses, H.: Atmospheric Radon-222 concentration variation with height and time, J. Appl. Meteorol., 5, 175-181, 1966. 8919
Petersen, A. C. and Holtslag, A. A. M.: A first-order closure for covariances and fluxes of reactive species in the convective boundary layer, J. Appl. Meteorol., 38, 1758–1776, 1999. 8920
Petersen, A. C., Beets, C., van Dop, H., and Duynkerke, P. G.: Mass-flux schemes for transport of non-reactive and reactive scalars in the convective boundary layer, J. Atmos. Sci., 56, 37–56, 1999. 8920
Petersen, A. C.: The impact of chemistry on flux estimates in the convective boundary layer, J. Atmos. Sci., 57, 3398–3405, 2000. 8920
Polian, G., Lambert, G., Ardouin, B., and Jegou, A.: Long-range transport of continental radon in subantarctic and antarctic areas, Tellus 38B, 178-189, 1986. 8919
Porstendörfer, J.: Properties and behaviour of radon and thoron and their decay products in the air, J. Atmos. Sci., 25, 219–263, 1994. 8919
Ramonet, M., Le Roulley, J. C., Bousquet, P., and Monfray, P.: Radon-222 measurements during the Tropoz II campaign and comparison with a global atmospheric transport model, J. Atmos. Chem., 23, 107-136, 1996. 8919
Robé, M. C., Rannou, A., and Le Bronec, J.: Radon measurement in the environment in France, Rad. Prot. Dos., 45, 455-457, 1992. 8919
Schumann, U.: Large-eddy simulation of turbulent diffusion with chemical reactions in the convective boundary layer, Atmos. Environ., 23, 1713–1729, 1989. 8920, 8925
Sykes, R. I., Parker, S. F., Henn, D. S., and Lewellen, W. S.: Turbulent mixing with chemical reactions in the planetary boundary layer, J. Appl. Meteorol., 33, 825–834, 1994. 8920, 8929
Sesana, L., Barbieri, L., Facchini, U., and Marcazzan, G. M.: 222Rn as a tracer of atmospheric motions: a study in Milan, Rad. Prot. Dos., 78, 65–71, 1998. 8919
Sesana, L., Ottobrini, B., Polla, G., and Facchini, U.: 222Rn as indicator of atmospheric turbulence: measurements at Lake Maggiore and on the pre-Alps, J. Env. Rad., 86, 271–288, 2006. 8919
Siebesma, A. P. and Cuijpers, J. W. M.: Evaluation of parametric assumptions for shallow

cumulus convection, J. Atmos. Sci., 52, 650–666, 1995. 8924
Stockwell, D. Z., Kritz, M. A., Chipperfield, M. P., and Pyle, J. A.: Validation of an off-line three dimensional chemical transport model using observed radon profiles - 2. Model results, J. Geophys. Res., 103, 8433-8445, 1998. 8919
van Zanten, M., Duynkerke, P. G., and Cuijpers, J. W. M.: Entrainment parameterizations in convective boundary layers, J. Atmos. Sci., 56, 813-828, 1999. 8934
Verver, G. H. L., van Dop, H., and Holtslag, A. A. M.: Turbulent mixing of reactive gases in the convective boundary layer, Bound.-Layer Meteorol., 85, 197–222, 1997. 8920
Vilà-Guerau de Arellano, J. and Cuijpers, J. W. M.: The chemistry of a dry cloud: the effects of radiation and turbulence, J. Atmos. Sci., 57, 1573–1584, 2000. 8924
Vilà-Guerau de Arellano, J.: Bridging the gap between atmospheric physics and chemistry in studies of small-scale turbulence, Bull. Amer. Meteor. Soc., 84, 51–56, 2003. 8925
Vinod Kumar, A., Sitaraman, V., Oza, R. B., and Krishamoorthy, T. M.: Application of a numerical model for the planetary boundary layer to the vertical distribution of radon and its daughter products, Atmos. Environ., 33, 4717–4726, 1999. 8919, 8920
Vinuesa, J.-F. and Vilà-Guerau de Arellano, J.: Fluxes and (co-)variances of reacting scalars in the convective boundary layer, Tellus 55B, 935-949, 2003. 8920, 8926, 8929
Vinuesa, J.-F. and Vilà-Guerau de Arellano, J.: Introducing effective reaction rates to account for the inefficient mixing of the convective boundary layer, Atmos. Environ., 39, 445–461, 2005. 8920
Wilkening, M. H.: Radon 222 concentrations in the convective patterns of a mountain environment, J. Geophys. Res., 75, 1733–1740, 1970. 8919
Wyngaard, J. C. and Brost, R. A.: Top-down and bottom-up diffusion of a scalar in the convective boundary layer, J. Atmos. Sci., 41, 102–112, 1984. 8928
Wyngaard, J. C.: Structure of the planetary boundary layer and implications for its modeling, J. Clim. App. Meteorol., 24, 1131–1142, 1985. 8920, 8928
Zahorowski, W., Chambers, S. D., and Henderson-Sellers, A.: Ground based radon-222 observations and their application to atmospheric studies, J. Env. Rad., 76, 3-33, 2004. 8919

Table 1. Initial values and prescribed surface fluxes used for both simulations.

	Steady-state CBL	Unsteady CBL
	(1)	(2)
z_i	662.5 m	187.5 m
Θ_m	288 K	286 K
$\Delta\Theta$	5 K	
$(\overline{w\theta})_s$	0.052 K m s^{-1}	
γ_θ	6 10^{-3} K m^{-1}	

ACPD
6, 8917–8960, 2006

Table 2. Volume averages of the turbulent Damköhler numbers.

Radioactive compounds	Steady-state CBL	Unsteady CBL
S_0	<0.01	<0.01
S_1	2.71	1.21–2.24
S_2	0.31	0.14–0.25
S_3	0.36	0.16–0.30

ACPD
6, 8917–8960, 2006

EGU

Table 3. Volume averages of the flux turbulent Damköhler numbers.

Radioactive compounds	Steady-state CBL	Unsteady CBL
S_0	<0.01	<0.01
S_1	1.08	0.62–0.38
S_2	0.85	0.06–0.09
S_3	0.16	0.01–0.02
S_4	<0.01	<0.01

ACPD
6, 8917–8960, 2006

EGU

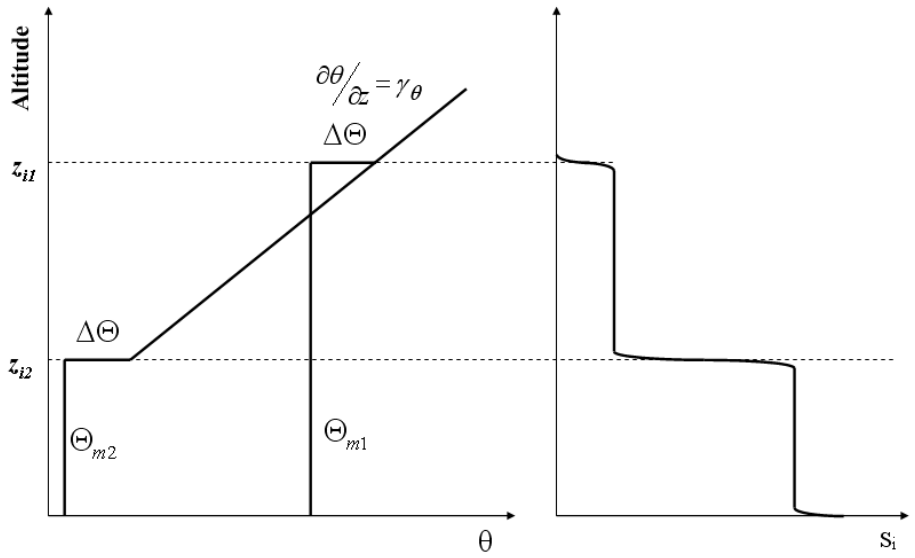

Fig. 1. Schematic representation of the experimental set-ups for the mean potential temperature Θ_m (1- steady state and 2- unsteady simulations) and the mean S_i concentration in the unsteady CBL simulation (see the text for a definition of the different quantities shown above).

ACPD
6, 8917–8960, 2006

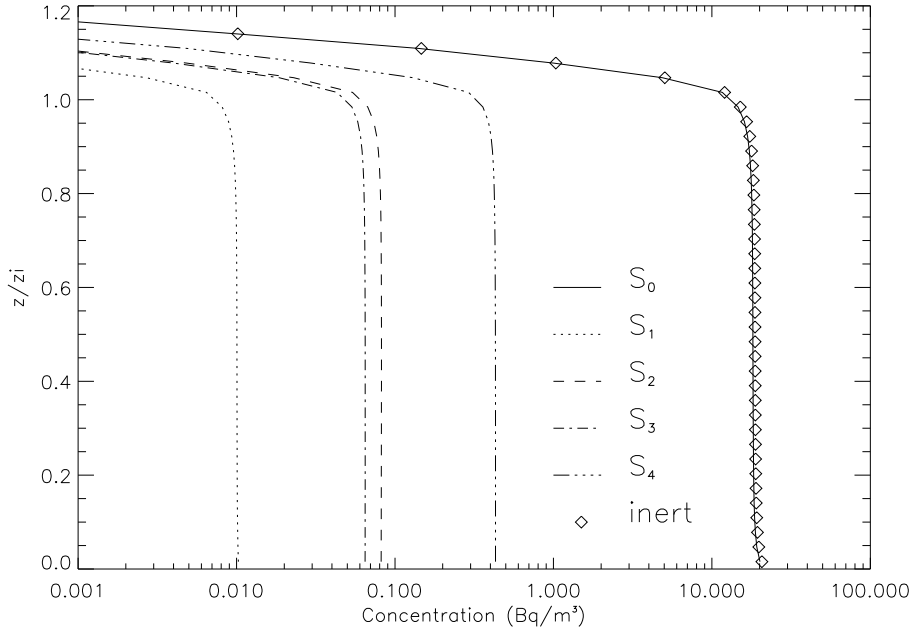

Fig. 2. Vertical profiles of ^{222}Rn and its progeny concentrations. The legend numbers represent the rank of the decaying compound in the radioactive decay chain. The diamonds account for the concentration of an inert scalar emitted at the surface with the same flux as ^{222}Rn.

ACPD
6, 8917–8960, 2006

EGU

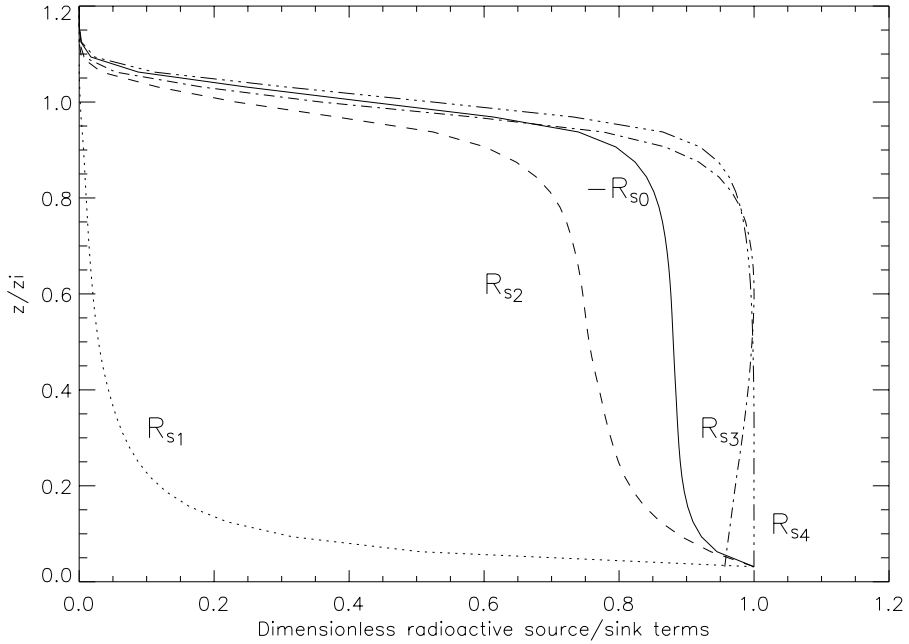

Fig. 3. Vertical profiles of the radioactive decay contribution to the concentration budget equations. The profiles are made dimensionless by using their maximum value. Note that the minus decay term of the ^{222}Rn concentration budget is plotted to increase readability.

ACPD
6, 8917–8960, 2006

EGU

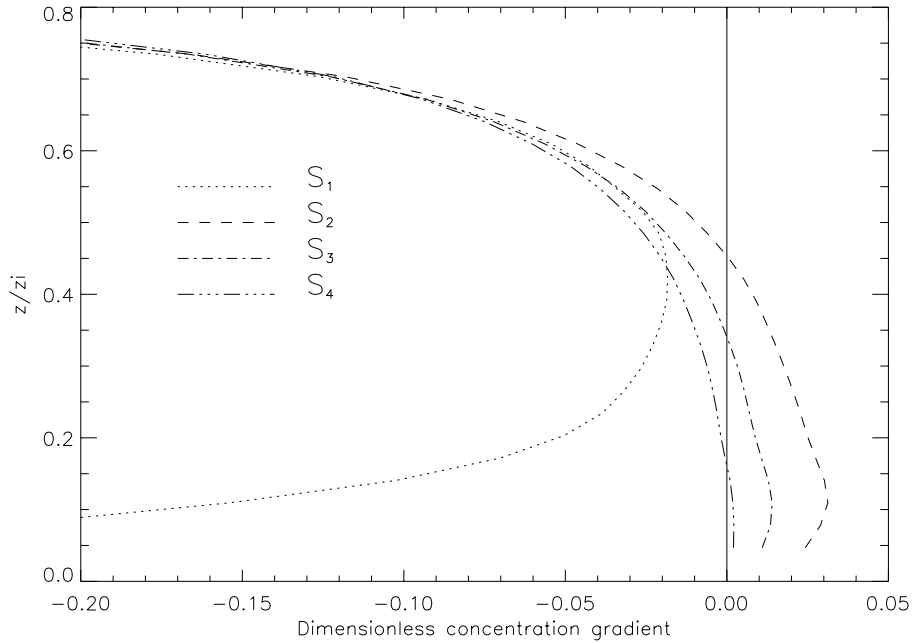

Fig. 4. Vertical profiles of the dimensionless concentration gradient of ^{222}Rn short-lived daughters S_1, S_2, S_3 and S_4. The profiles are scaled with the daughters' maximum CBL concentration and made dimensionless by z_i. To increase readability, only the part of the CBL where discrepant profiles are found is shown.

ACPD
6, 8917–8960, 2006

EGU

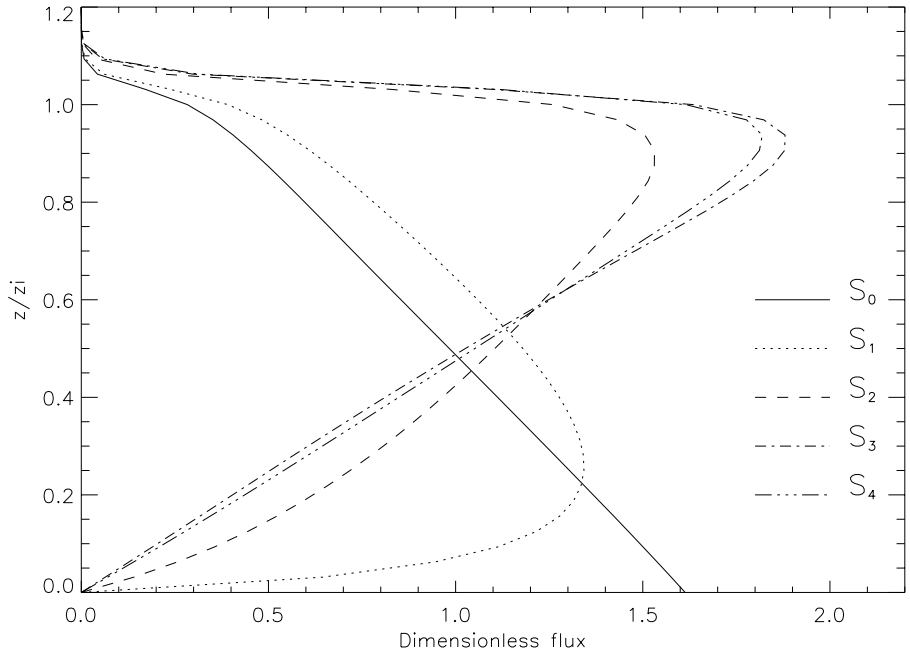

Fig. 5. Vertical profiles of the dimensionless fluxes for ^{222}Rn and its daughters. The values are made dimensionless by $w_* s_{i_*}$ as proposed by Cuijpers and Holtslag (1998).

ACPD
6, 8917–8960, 2006

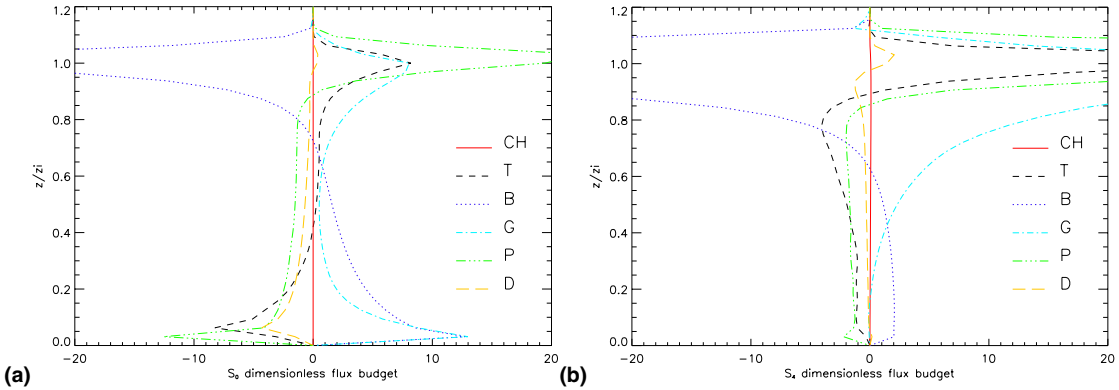

Fig. 6. Vertical profiles of the different contributions flux budget equations of **(a)** ^{222}Rn (S_0) and **(b)** ^{210}Pb (S_4). The profiles are made dimensionless using $w_*^2 s_{i*} z_i^{-1}$.

ACPD
6, 8917–8960, 2006

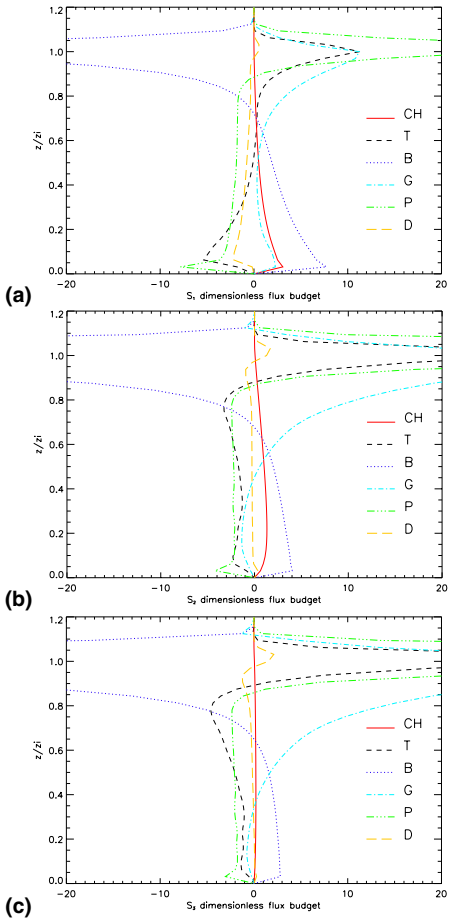

Fig. 7. Vertical profiles of the contributions to the flux budget equations of **(a)** ^{218}Po (S_1), **(b)** ^{214}Pb (S_2) and **(c)** ^{214}Bi (S_3). The profiles are made dimensionless using $w_*^2 s_{i*} z_i^{-1}$.

ACPD
6, 8917–8960, 2006

EGU

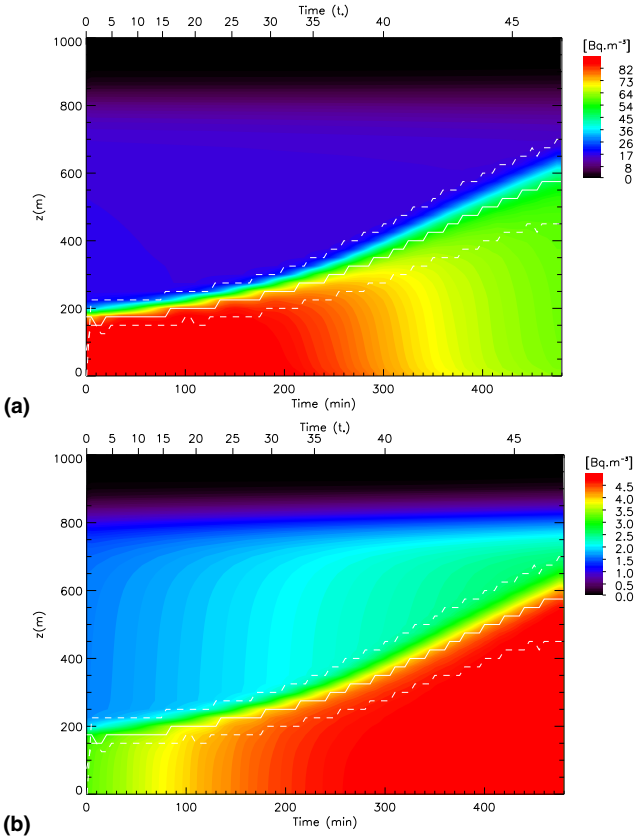

Fig. 8. Vertical profiles of **(a)** ^{222}Rn (S_0) and **(b)** ^{210}Pb (S_4) concentrations. The top of the CBL is overplotted with a white solid line and the entrainment layer is located between the dashed white lines. The steppy aspect of these latter quantities is due to averaging procedures, e.g. the CBL depth and the entrainment layer locations are determined from the 5 min slab averaged sensible heat flux. The concentrations are plotted against time in minutes (lower x-axis) and in t_* (upper x-axis) where $t_*=z_i/w_*$.

ACPD
6, 8917–8960, 2006

EGU

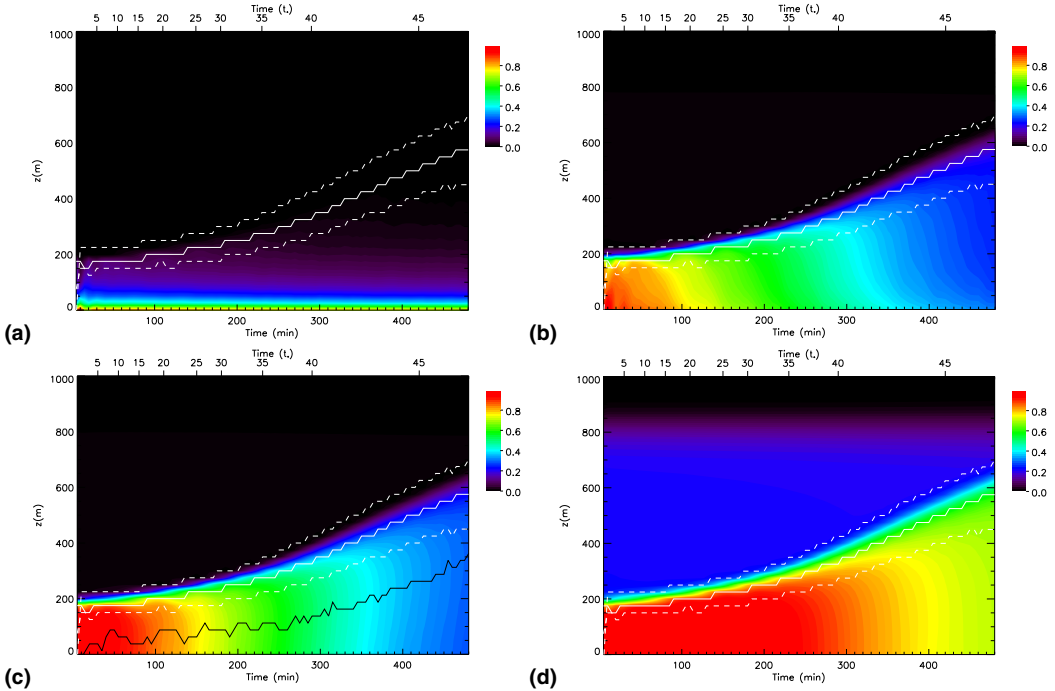

Fig. 9. Vertical profiles of the radioactive decay contributions to ^{222}Rn progeny concentrations. Subfigures **(a)**, **(b)**, **(c)** and **(d)** are showing R_{S_1}, R_{S_2}, R_{S_3} and R_{S_4}, respectively. The top of the CBL is overplotted with a white solid line and the entrainment layer is located between the dashed white lines. As in Fig. 8, the steppy aspect of these latter quantities is due to the time averaging procedure. The location of the R_{S_3} maximum is also shown with a solid black line. The contributions have been made dimensionless using their maximum values. The profiles are plotted against time in minutes (lower x-axis) and in t_* (upper x-axis) where $t_*=z_i/w_*$.

ACPD
6, 8917–8960, 2006

EGU

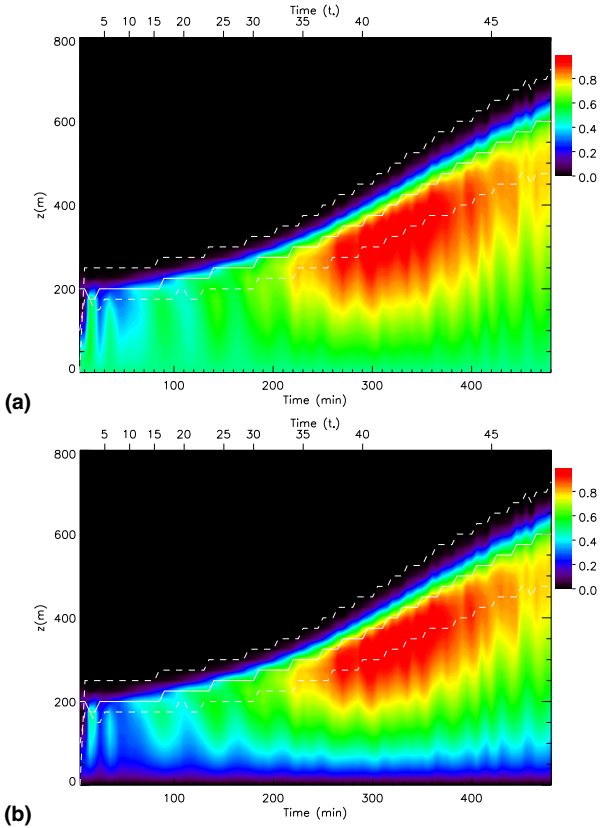

Fig. 10. Vertical profiles **(a)** ^{222}Rn (S_0) and **(b)** ^{218}Po (S_1) instantaneous fluxes. The fluxes are made dimensionless using their maximum values. The top of the CBL is overplotted with a white solid line and the entrainment layer is located between the dashed white lines. As in Figs. 8 and 9, the steppy aspect of these latter quantities is due to the time averaging procedure. The fluxes have been made dimensionless using their maximum values. The profiles are plotted against time in minutes (lower x-axis) and in t_* (upper x-axis) where $t_*=z_i/w_*$.

ACPD
6, 8917–8960, 2006

EGU

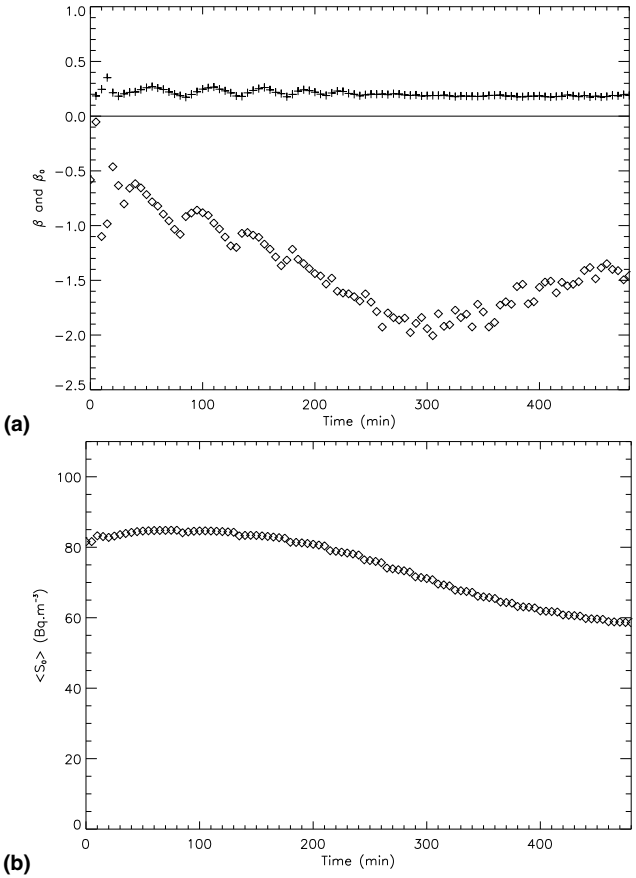

Fig. 11. Time evolution of **(a)** the ratios of the entrainment flux to the surface flux for potential temperature (crosses) and ^{222}Rn (diamonds), and **(b)** ^{222}Rn mixed-layer concentration $<S_0>$.

ACPD
6, 8917–8960, 2006

EGU